Int J Earth Sci (Geol Rundsch)
DOI 10.1007/s00531-012-0772-5

ORIGINAL PAPER

Zircon response to high-grade metamorphism as revealed by U–Pb and cathodoluminescence studies

W. Siebel · C. K. Shang · E. Thern · M. Daniš́k · J. Rohrmüller

Received: 30 March 2011 / Accepted: 28 March 2012

Abstract Correct interpretation of zircon ages from high-grade metamorphic terrains poses a major challenge because of the differential response of the U–Pb system to metamorphism, and many aspects like pressure–temperature conditions, metamorphic mineral transformations and textural properties of the zircon crystals have to be explored. A large (c. 450 km^2) coherent migmatite complex was recently discovered in the Bohemian Massif, Central European Variscides. Rocks from this complex are characterized by granulite- and amphibolite-facies mineral assemblages and, based on compositional and isotopic trends, are identified as the remnants of a magma body derived from mixing between tonalite and supracrustal rocks. Zircon crystals from the migmatites are exclusively large (200–400 μm) and yield ^{207}Pb/^{206}Pb evaporation ages between 342–328 Ma and single-grain zircon fractions analysed by U–Pb ID-TIMS method plot along the concordia curve between 342 and 325 Ma. High-resolution U–Pb SHRIMP analyses substantiate the existence of a resolvable age variability and yield older ^{206}Pb/^{238}U ages (342–330 Ma, weighted mean age = 333.6 ± 3.1 Ma) for inner zone domains without relict cores and younger ^{206}Pb/^{238}U ages (333–320 Ma, weighted mean age = 326.0 ± 2.8 Ma) for rim domains. Pre-metamorphic cores were identified only in one sample (^{206}Pb/^{238}U ages at 375.0 ± 3.9, 420.3 ± 4.4 and 426.2 ± 4.4 Ma). Most zircon ages bracket the time span between granulite-facies metamorphism in the Bohemian Massif (~345 Ma) and the late-Variscan anatectic overprint (Bavarian phase, ~325 Ma). It is argued that pre-existing zircon was variously affected by these metamorphic events and that primary magmatic growth zones were replaced by secondary textures as a result of diffusion reaction processes and replacement of zircon by dissolution and recrystallization followed by new zircon rim growth. Collectively, the results show that the zircons equilibrated during high-grade metamorphism and record partial loss of radiogenic Pb during post-peak granulite events and new growth under subsequent anatectic conditions.

Keywords Bohemian Massif · Granulite-facies · Migmatite · U–Pb zircon · Variscides

W. Siebel (✉) · C. K. Shang
Fachbereich Geowissenschaften, University of Tübingen, 72074 Tübingen, Germany
e-mail: wolfgang.siebel@uni-tuebingen.de

E. Thern
Curtin University of Technology, Perth, WA 6845, Australia

M. Daniš́k
University of Waikato, Hamilton 3240, New Zealand

J. Rohrmüller
Bayerisches Landesamt für Umwelt, 95615 Marktredwitz, Germany

Introduction

Numerous studies have highlighted the chemical durability of zircon to intracrustal recycling and metamorphism (for reviews see Mezger and Krogstad 1997; Scherer et al. 2007). Resistance to Pb diffusion during orogenic cycles gives zircon a unique capacity among geochronometers and allows scientists to observe ancient crust-forming periods in zircons collected from much younger rocks (Wilde et al. 2001). Once formed, zircons can sustain mantle storage (Siebel et al. 2009), crustal recycling and melt–peridotite interaction (Liu et al. 2010) or subduction/exhumation and eclogite-facies metamorphism (Rubatto and Scambelluri

Published online: 22 April 2012

2003). Zircons have also been shown to survive crustal anatexis and high-temperature granulite-facies metamorphism (Connelly 2001; Möller et al. 2002; Zeck and Williams 2002; Whitehouse and Platt 2003; Crowley et al. 2008). The paper by Möller et al. (2002) on granulites from SW Norway has demonstrated that the U–Pb isotope system in zircons was not completely reset during a thermal overprint of c. 950 °C. However, Guo et al. (2005) came up with results that cast some doubt on the robustness of the U–Pb zircon system. In mafic granulites from the North China craton, they encountered zircon populations that postdate the time of magmatism by c. 700 Ma. Their results suggest that U–Pb isotopic signatures of these zircons were completely obliterated by later high-grade metamorphism. It was also reported that during granulite-facies metamorphism, whole new zircon grains with magmatic features can form if a melt phase is present (Roberts and Finger 1997; Schaltegger et al. 1999). An operative mechanism of zircon formation in the presence of an aqueous fluid or melt phase is re-equilibration by an interface-coupled dissolution–precipitation process that operates at an inwardly moving reaction front (Geisler et al. 2007; Harley et al. 2007; Soman et al. 2010). These studies imply differential behaviour of the U–Pb system during granulite-facies metamorphism. Central to this debate is the need to find a natural example that helps to illustrate the zircon response to metamorphism. Here, we elaborate the fate of zircons from an ortho-derivative granulite-facies migmatite complex that was recently discovered in the Bohemian Massif (Propach et al. 2008). We demonstrate that most of the zircon ages, in spite of defining a coherent data set, do not reflect the primary zircon crystallization from a melt. The results of our study suggest that primary magmatic zircon was almost completely transformed and modified followed by later precipitation of new zircon during two high-grade metamorphic events.

Geological setting and fundamental problems

The newly identified migmatite complex is located in the SW Bohemian Massif, between the Danube fault and the Pfahl shear zone, southern Bavarian Forest (Fig. 1). This area belongs to the innermost part (Moldanubian zone) of the Variscan orogenic belt in central Europe. The Moldanubian zone can be subdivided into a structurally lower Monotonous Group, a structurally intermediate Varied Group and a structurally higher Gföhl Group (Schulmann et al. 2005).

The Monotonous Group is dominated by a several-km-thick uniform areno-argillaceous greywacke series, now transferred into migmatitic and anatectic biotite-plagioclase

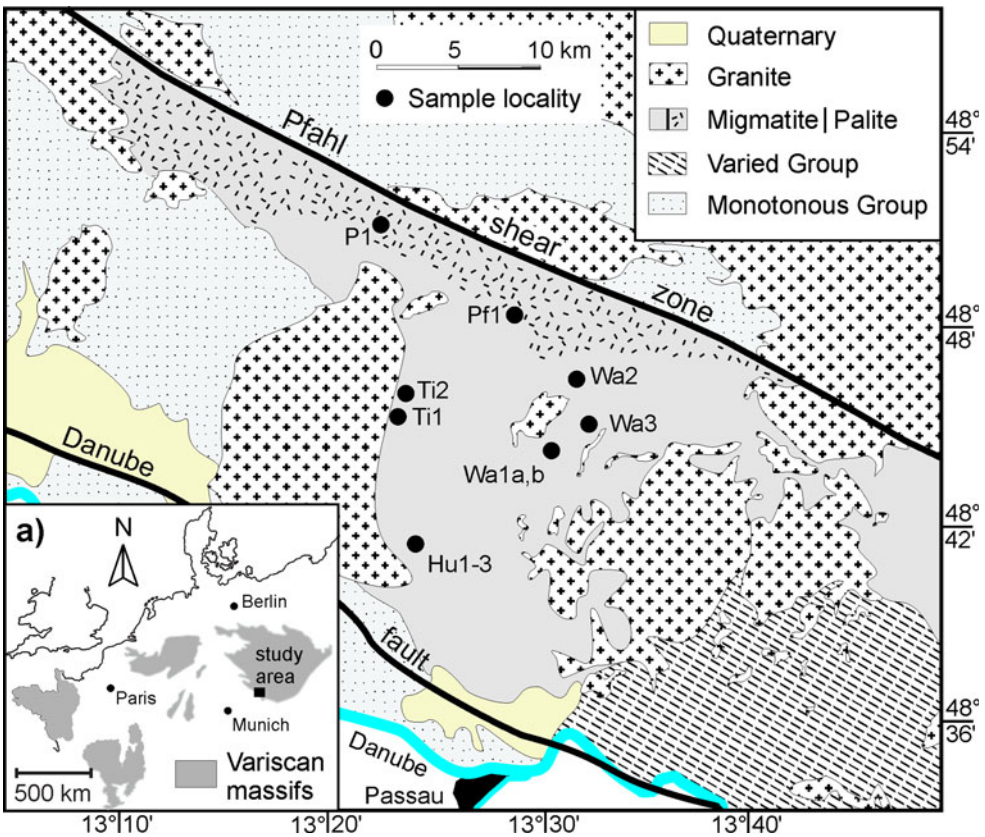

Fig. 1 **a** Location map of the Bohemian Massif and study area (*black square*) in central Europe, and **b** *geological map* showing the distribution of the migmatite complex of the Bavarian Forest and sample localities

paragneisses. Neoproterozoic–Early Palaeozoic sedimentation was assigned for this sequence (Gebauer et al. 1989; Kröner et al. 1988). Metafelsic and metabasic intrusions of Neoproterozoic and Ordovician age are interleaved within the sedimentary succession (Teipel et al. 2004). The Varied Group consists of a presumably Early Palaeozoic metasedimentary sequence, which includes quartzites, graphite schists, calc-silicate rocks, as well as metabasic igneous rocks (Janoušek et al. 2008; Schulmann et al. 2009). The Gföhl Group is made up of high-grade metamorphic rocks (eclogites, granulites, amphibolites, migmatites, ultramafics) and orthogneisses with Ordovician and Devonian protolith ages (Friedl et al. 2004; Kröner et al. 2000). The Gföhl and the Varied Groups have been considered as tectonically emplaced (allochthonous) units, and contacts between these units and the Monotonous Group are interpreted as shear horizons (Fiala et al. 1995; Franke 2000).

During the Lower Carboniferous (i.e. 355–345 Ma), large parts of the Moldanubian zone, in particular rocks of the Gföhl and Varied Groups, were subjected to Variscan granulite-facies metamorphism (Carswell and O'Brian 1993; Finger et al. 2007). The south-western margin of the Bohemian Massif, including the study area, was ultimately affected by another high-temperature metamorphic event (Bavarian phase). Petrological work indicates pressure and temperature conditions of 700–850 °C and c. 4–5 kbar (Kalt et al. 2000) for this thermal overprint, which was superimposed by major granite intrusions around 328–321 Ma (Siebel et al. 2008).

The migmatite/orthoanatexite complex of the southern Bavarian Forest is sandwiched between the Monotonous Group and the Varied Group (or Kropfmühl series; for rock description, see Finger et al. 2007). Towards the Pfahl zone (Fig. 1b), the complex grades into a zone of feldspar-phyric ortho-derivative rocks. In the older literature, this rock-type is referred to as *palite* (Frentzel 1911). The term 'palite' was used for coarse-grained, inequigranular granitoids of dominantly granodioritic composition, which often contain large augen-shaped megacrysts of K-feldspar, and numerous mafic enclaves. Lithological and geochemical similarities between the migmatites and the palites imply a similar tectonomagmatic evolution of both units (Propach et al. 2008). A close genetic relationship between these two units is also indicated by radiometric age data. Zircon ages from two palite samples (Pb evaporation data; Siebel et al. 2005a, b) and one orthoanatexite sample (U–Pb SHRIMP data; Finger et al. 2010) span an identical approximate age range (~345–325 Ma). In either case, the data provide ample evidence for two episodes of zircon growth. The older ages were interpreted as formation ages of the igneous protoliths whereas the younger ages are regarded to reflect the final metamorphic overprint (Finger et al. 2010). Straightforward interpretation in terms of protolith ages may be questioned with regard to the complex metamorphic evolution of this terrane. During the late-Variscan Bavarian phase, the rocks were transferred into migmatites and anatexites (Propach et al. 2008; Finger et al. 2010 and references therein). Several localities with relict granulite-facies mineral assemblages and metamorphic reaction textures have been identified within the migmatite complex, and this was taken as evidence for an older high-grade metamorphic event (Propach et al. 2008). Thus, it has to be assumed that the rocks were affected by two distinct cycles of metamorphism—an earlier granulite-facies metamorphism and a later amphibolite-facies metamorphism. If the granulite-facies assemblage of the migmatites/orthoanatexites formed during Early Carboniferous regional high-pressure metamorphism, as in southern Bohemia (Kröner et al. 2000; Wendt et al. 1994), the intrusion of the original igneous protolith is most likely pre-Carboniferous in age.

Analytical methods

Sample preparation—geochemistry

Investigations were carried out on ten orthoanatexite samples collected from different quarries or road cuts. Additionally, a sample from a garnet-bearing granulite-facies enclave (sample Ti2, Table 1) was analysed. All samples were collected from fresh rock surfaces. Sample locations are plotted in Fig. 1b, and the co-ordinates of our sampling sites are given in Table 1.

Unless otherwise stated, all analyses were conducted at the Tübingen geosciences faculty. Rock fragments were crushed in a jaw breaker and powdered in an agate mill. Pure zircon fractions from the orthoanatexites and a garnet fraction from the granulite enclave were obtained by standard mineral separation techniques, including a Wilfley table, a Frantz isodynamic separator, heavy liquids and final selection by handpicking under a binocular microscope. Cathodoluminescence (CL) imaging of polished zircon grains was carried out on a JEOL JXA-8900RL electron-microprobe working with an accelerating voltage of 15 kV and a beam current of 15 nA.

Whole-rock major and trace element compositions were determined by wavelength X-ray fluorescence (XRF) spectrometry on a Bruker AXS S4 pioneer spectrometer, following standard analytical techniques (Potts and Webb 1992). Major elements and most trace elements were measured on fused glass beads made from whole-rock powder (1.50 g) mixed with 7.50 g of Spectromelt fluxing agent. Loss on ignition (LOI) was calculated after heating the sample powder to 1,050 °C for 1 h. Analytical uncertainties range from 1–5 % and 5–10 % for major and trace

Table 1 Geochemical and Sr–Nd isotopic composition of samples from the migmatite complex

Geographic coordinates	Hu1 48°41′ 42″N 13°23′7″E	P1 48°50′ 38″N 13°22′11″E	Wa2 48°45′ 48″N 13°36′25″E	Wa1a 48°46′ 11″N 13°30′34″E	PF1 48°47′ 33″N 13°30′22″E	Ti1 48°45′ 23″N 13°22′33″E	Wa3 48°44′ 56″N 13°36′31″E	Hu2 48°41′ 42″N 13°23′7″E	Wa1b 48°46′ 11″N 13°30′34″E	Hu3 48°41′ 42″N 13°23′7″E	Ti2[a] 48°45′ 46″N 13°23′8″E
SiO_2	54.65	58.70	59.40	60.37	62.10	63.84	64.05	66.94	67.82	71.65	66.01
TiO_2	1.90	1.06	0.93	0.92	0.78	0.46	0.78	0.38	0.77	0.41	0.89
Al_2O_3	16.74	18.20	17.52	16.15	16.50	16.77	14.66	17.31	14.09	14.54	16.82
Fe_2O_3	7.66	5.46	8.68	6.14	4.57	3.83	5.38	3.10	5.36	2.32	7.13
MnO	0.09	0.05	0.18	0.08	0.07	0.07	0.07	0.06	0.08	0.04	0.10
MgO	4.34	2.75	2.98	3.99	2.38	2.46	3.33	1.24	2.67	0.81	2.30
CaO	4.01	4.61	1.57	3.35	3.56	3.73	2.89	3.54	3.80	3.10	0.75
Na_2O	3.26	3.97	2.58	3.26	3.34	3.81	2.71	4.27	3.43	3.63	1.59
K_2O	5.56	3.97	4.61	4.36	4.41	4.12	4.64	3.31	1.45	2.83	3.46
P_2O_5	0.99	0.47	0.07	0.48	0.32	0.29	0.31	0.14	0.04	0.07	0.10
LOI[b]	0.91	0.82	0.78	0.90	1.34	0.50	1.69	0.36	0.62	0.36	0.97
Sum	100.11	99.20	99.30	100.00	98.00	99.88	100.51	100.65	100.13	99.76	100.12
ASI[c]	0.90	0.95	1.45	1.00	0.99	0.96	0.99	1.02	1.00	0.99	2.18
Ba	2,319	1,108	1,711	1,016	1,107	1,603	1,232	989	222	749	1,093
Rb	198	187	139	187	158	144	164	91	68	81	96
Sr	528	567	326	325	456	725	283	517	291	401	216
V	167	82	138	105	78	44	80	34	64	28	101
Y	47	29	76	39	21	17	20	40	22	10	46
Zr	329	473	395	416	361	234	240	217	467	166	267
Zn	96	80	80	83	77	43	58	23	64	9	62
Cr	50	73	113	146	56	78	134	9	114	8	84
Ni	104	31	106	123	9	63	102	55	126	33	100
Nb	28	39	18	30	32	–	–	–	24	–	20
Ce	150	104	134	189	76	117	48	61	76	43	98
La	27	43	45	86	34	65	14	37	44	30	37
Nd	63	53	55	75	37	50	26	20	34	22	45
Sm	8.8	7.0	8.7	10.9	4.7	8.2	4.4	3.8	4.7	2.5	6.6
Eu	1.7	1.2	1.4	1.4	1.2	2.1	0.9	1.4	1.1	1.0	1.1
Yb	3.8	2.1	6.7	3.0	1.5	1.3	1.6	1.1	1.2	0.8	4.1
T_{Zr} (°C)[d]	792	844	887	845	835	793	803	799	874	782	890
M[e]	2.17	1.93	1.22	1.77	1.72	1.76	1.66	1.59	1.57	1.50	0.72
$^{87}Rb/^{86}Sr$	1.123	0.937	1.335	1.799	0.941	0.618	1.765	0.540	0.703	0.608	1.389
$^{87}Sr/^{86}Sr \pm 2\sigma_{measured}$	0.711076 ± 10	0.711941 ± 9	0.719247 ± 10	0.721897 ± 10	0.712314 ± 10	0.711249 ± 7	0.718964 ± 10	0.707075 ± 10	0.712286 ± 10	0.708283 ± 10	0.721166 ± 10
$(^{87}Sr/^{86}Sr)_i^f$	0.70564	0.70754	0.71278	0.71319	0.70789	0.70826	0.71042	0.70446	0.70888	0.70534	0.71445
$^{147}Sm/^{144}Nd$	0.1119	0.1084	0.0763	0.0990	0.1043	0.0970	0.1253	0.1076	0.0766	0.0976	0.1093

Table 1 continued

Geographic coordinates	Hu1 48°41′ 42″N 13°23′7″E	P1 48°50′ 38″N 13°22′11″E	Wa2 48°45′ 48″N 13°36′25″E	Wa1a 48°46′ 11″N 13°30′34″E	PF1 48°47′ 33″N 13°30′22″E	Ti1 48°45′ 23″N 13°22′33″E	Wa3 48°44′ 56″N 13°36′31″E	Hu2 48°41′ 42″N 13°23′7″E	Wa1b 48°46′ 11″N 13°30′34″E	Hu3 48°41′ 42″N 13°23′7″E	Ti2[a] 48°45′ 46″N 13°23′8″E
$^{143}Nd/^{144}Nd \pm 2\sigma_{measured}$	0.512361 ± 7	0.512230 ± 10	0.511915 ± 9	0.512025 ± 10	0.512202 ± 10	0.512204 ± 8	0.512186 ± 30	0.512277 ± 9	0.512108 ± 10	0.512284 ± 9	0.511884 ± 10
$(^{143}Nd/^{144}Nd)_i$[f]	0.512112	0.511989	0.511745	0.511804	0.511970	0.511988	0.511907	0.512038	0.511937	0.512066	0.511641
$\varepsilon Nd_{(t)}$	−1.7	−4.2	−8.9	−7.7	−4.6	−4.1	−5.7	−3.2	−5.1	−2.6	−10.9
T_{DM}(Ga)	1.22	1.42	1.80	1.71	1.45	1.42	1.55	1.34	1.50	1.29	1.97

Data for samples P1 and PF1 from Siebel et al. (2005a, b). Major elements in wt% and trace element in ppm

– Below detection limit

[a] Granulite enclave

[b] Loss on ignition

[c] *ASI* alumina saturation index (mol% $[Al_2O_3/(CaO + Na_2O + K_2O)]$

[d] Zircon saturation temperature

[e] Cation ratio (Na + K + 2Ca)/(Al x Si)

[f] Initial ratios calculated using the age 340 Ma

elements, respectively, depending on the concentration level.

Sr–Nd isotope analyses

For Rb–Sr and Sm–Nd isotope analyses, samples were spiked with ^{150}Nd-^{149}Sm and ^{87}Rb-^{84}Sr tracer solutions prior to dissolution in hydrofluoric acid at 180 °C in pressure digestion bombs. Rb, Sr and the light rare earth elements were isolated from each other by standard ion-exchange chromatography (Crock et al. 1984) with a 5-ml resin bed of AG 50 W-X12 (200–400 mesh). Nd and Sm were separated on quartz columns using 1.7 ml Teflon powder coated with HDEHP, di (2-ethylhexyl) orthophosphoric acid, as cation-exchange medium (Richard et al. 1976). Isotopic data were obtained in static mode on a Finigan MAT 262 mass spectrometer. The $^{143}Nd/^{144}Nd$ ratios were normalized to $^{146}Nd/^{144}Nd = 0.7219$, and the $^{87}Sr/^{86}Sr$ isotope ratios to $^{86}Sr/^{88}Sr = 0.1194$. Repeated measurements of the LaJolla Nd standard ($n = 12$) yielded a $^{143}Nd/^{144}Nd$ ratio of 0.511844 ± 13 (errors are ± 2σ of the mean) while ten analyses of the NBS 987 Sr standard yielded a mean value of $^{87}Sr/^{86}Sr = 0.710238 \pm 0.000014$, in good agreement with the certified values of 0.511860 (LaJolla) and 0.710248 (NBS 981). Total procedural blanks were 100 pg for Nd and 220 pg for Sr. εNd values were calculated using present-day CHUR values of 0.1967 for $^{147}Sm/^{144}Nd$ (Jacobsen and Wasserburg 1980) and 0.512638 for $^{143}Nd/^{144}Nd$ (Goldstein et al. 1984).

TIMS and single zircon evaporation technique

For U–Pb analyses, zircons were cleaned with 6 N HCl and ultra-pure H_2O, and a mixed ^{205}Pb-^{235}U tracer solution was added to the grains prior to pressure dissolution in 22 N HF. A subset of zircon fractions was submitted to a thermal annealing experiment (1,000 °C, 48 h) after Mattinson (2005). Separation and purification of uranium and lead were performed in small Teflon columns, filled with 40 µl of Bio-Rad AG1-X8 resin, using standard ion-exchange separation techniques as described by Manhès et al. (1978). Uranium and lead isotopic measurements were carried out on a Finnigan MAT 262 multi-collector mass spectrometer in single Re filament mode using silica-gel activator. Total procedure blanks were <10 pg for lead and uranium. U–Pb age parameters were calculated using the ISOPLOT program (Ludwig 2003).

For Pb evaporation analyses, single zircon grains were embedded into a Re evaporation filament and measured on a Finnigan MAT 262 mass spectrometer equipped with a single secondary electron multiplier (SEM). The analytical procedures are described elsewhere (e.g. Kober 1987; Klötzli 1997; Siebel et al. 2003). From each zircon grain,

lead from 2 to 4 different heating/evaporation steps was analysed, and the mean of the ^{204}Pb corrected radiogenic ^{207}Pb/^{206}Pb ratio from all steps was calculated if the data for the individual steps were concordant within the error. The age for several zircons from the same sample is given as weighted average, and the error refers to the 95 % confidence level (ISOPLOT, Ludwig 2003). The accuracy of the measurements was monitored by repeated measurement of the Plešovice zircon standard, which yielded a ^{207}Pb/^{206}Pb evaporation age of 335.3 ± 3.2 Ma ($n = 5$) and an upper intercept U–Pb zircon age of 337.3 ± 2.7 Ma, identical within the errors to the weighted mean ^{238}U/^{206}Pb age of 337.1 ± 0.4 Ma reported by Sláma et al. (2008).

SHRIMP analytical technique

Zircon grains together with grain fragments of standards were mounted in epoxy resin and polished to expose a surface suitable for in situ U-Th–Pb data acquisition. Zircons were analysed on the sensitive high-resolution ion microprobe (SHRIMP) at the John de Laeter Centre of Mass Spectrometry, Curtin University of Technology, Perth, Australia, using procedures similar to those described in Nelson (1997, 2001). Each analysis was comprised of six cycles measuring each of nine masses: $^{196}Zr_2O$ (2 s), ^{204}Pb (10 s), ^{204}Pb, background (10 s), ^{206}Pb (20 s), ^{207}Pb (40 s), ^{208}Pb (10 s), ^{238}U (5 s), ^{248}ThO (5 s) and ^{254}UO (2 s). Operating conditions for the session included a 2.8 nA O_2 primary beam, ~30 μm spot size and a mass resolution >4,500 R (1 % peak height, SHRIMP "A"). The Sri Lankan zircon M257 (Nasdala et al. 2008; ^{206}Pb/^{238}U age = 561.3 ± 0.3 Ma, 840 μg g^{-1} U, Th/U ~ 0.27) was used for U/Pb calibration and calculation of U and Th concentrations. During the SHRIMP session, seventeen analyses of M257 were measured and indicated a Pb/U calibration uncertainty of ± 1.049 % (1σ). SHRIMP data have been reduced using CONCH software (Nelson 2006). Common Pb corrections have been applied to all data using the ^{204}Pb correction method as described in Compston et al. (1984). Common Pb measured in standard analyses is considered to be derived from the gold coating and assumed to have an isotopic composition equivalent to Broken Hill common Pb (^{204}Pb/^{206}Pb = 0.0625, ^{204}Pb/^{206}Pb = 0.9618, ^{204}Pb/^{206}Pb = 2.2285; Cumming and Richards 1975).

Field and petrographic observations

The morphology of the migmatites varies considerably, and a complete range from metatexite to diatexite migmatitic structures has been produced during high-grade metamorphic processes (Fig. 2a). Typical gneisses are mesocratic to melanocratic and show medium-grain sizes. Gradation between foliated rocks and those that are dominantly granoblastic with homogeneous diatectic texture (Fig. 2b) are generally observed. Although pre-migmatitic protolith textures are disrupted or obliterated by anatectic overprint, the presence of mafic microgranular enclaves (amphibolites, minor ultramafics) still features their plutonic parentage and also attests that magma mixing occurred (Fig. 2c). The major mineral assemblage of the migmatite complex consists of plagioclase (20–50 %, and with An_{50}-An_{35}), K-feldspar (5–20 %), quartz (5–20 %), biotite (5–30 %), amphibole (3–20 %) and clino- and orthopyroxene (0–20 %). Garnet is only present in some leucocratic migmatite varieties (sample Wa-2) and in the granulite enclave sample Ti2. Accessory phases are apatite, titanite, zircon, epidote, magnetite and sulphide minerals.

At microscopic scale, some rocks provide evidence for an orthopyroxene-bearing granulite-facies assemblage inferred to have formed by the following types of prograde mineral reactions: (1) biotite + quartz → orthopyroxene (hypersthene) + K-feldspar + H_2O and (2) biotite + quartz + amphibole → orthopyroxene + K-feldspar + plagioclase + H_2O (e.g. Humphreys and Cornell 1989). The orthopyroxene-in reaction, which involves the breakdown of hydrous minerals in quartz-bearing igneous rocks of intermediate composition, indicates granulite-facies conditions with temperatures exceeding 800 °C. In sample Wa1b (Fig. 2d), orthopyroxenes are typically mantled by thin (~100 μm) coronas of polycrystalline amphibole, a feature that has been related to decompression from granulite-facies (Grant et al. 2009). Some mafic granulites containing plagioclase + pyroxene ± biotite are found as enclaves in the migmatites, and a biotite + quartz + cordierite + garnet + K-feldspar + plagioclase ± sillimanite association of an enclave (sample Ti2) attests to pT-conditions of 4–8 kbar and 700–800 °C. In the northern sector of the migmatite complex (palite zone, Fig. 1b), granulite-facies assemblages have not been observed. This can be explained by strong anatectic recrystallization and metablastic coarsening of the rocks near the Bavarian Pfahl shear zone.

Geochemistry, Rb–Sr and Sm–Nd isotope systematics

Geochemical features of the migmatites have been documented in detail by Propach et al. (2008), and only a brief summary is provided here. Typically, these rocks have SiO_2 contents of 55–72 wt%, are metaluminous, have high potassium concentrations and are calc-alkaline in composition (Table 1). The samples are characterized by compositions ranging from tonalite, granodiorite through monzodiorite, monzonite to granite with intermediate

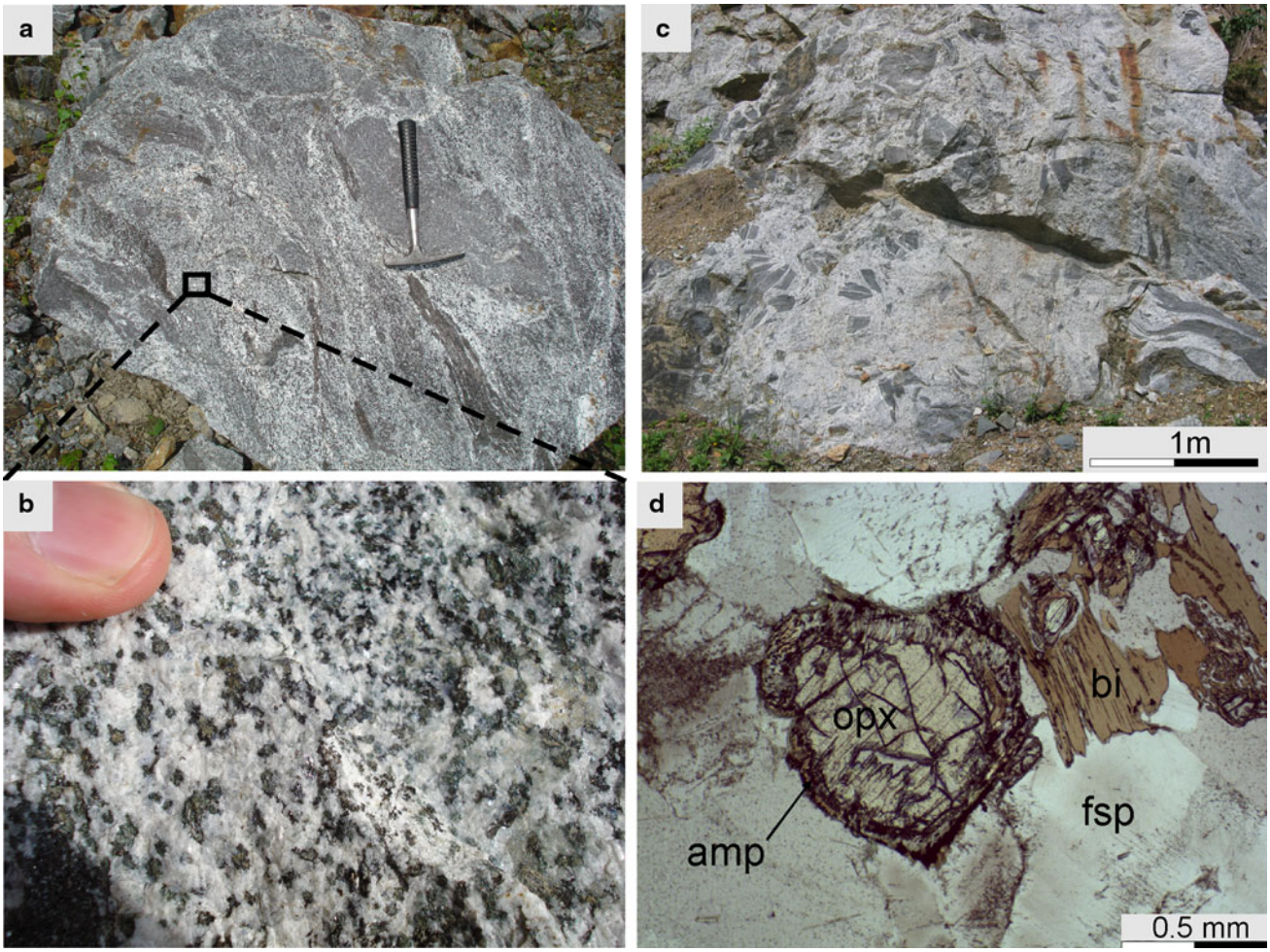

Fig. 2 Field appearance of typical rock types from the migmatite complex. **a** Large boulder with migmatitic appearance; **b** close-up of a more coarse-grained leucocratic part with homogenization of (pre-migmatitic) texture; **c** accumulation of pre-migmatitic enclaves in diatexite; **d** thin section photograph of migmatite sample Wa1b (pyroxene granulite) depicting a large orthopyroxene crystal mantled by amphibole

compositions being the most abundant. They are amphibole- and magnetite-bearing, I-type granitoids, enriched in light rare earth relative to heavy rare earth elements as well as in large ion lithophile elements and depleted in Ti and Nb. These are common compositional features of magmas associated with active plate margins. The concentrations of most major and trace elements decrease with increasing silica concentration, except for CaO and Na_2O, which portray no correlation with SiO_2.

The rocks show considerable isotope variation and negative correlation between $(^{87}Sr/^{86}Sr)_{340\ Ma}$ isotope ratios (0.7045–0.7132) and $\varepsilon Nd_{340\ Ma}$ values (−1.7 to −8.9) (Fig. 3; Table 1). Interestingly, samples with less-evolved isotopic composition have distinctively lower Fe_2O_3 and higher Na_2O concentrations compared with the isotopically more evolved samples (Fig. 3). The isotopically more evolved samples (e.g. Wa1a, Wa2 and Ti2: 1.7–2.0 Ga) have older crustal residence Nd model ages compared with the less-evolved members (1.2–1.5 Ga) (Table 1).

Sm–Nd analyses were carried out on garnet from the granulite enclave sample Ti2 (Table 2). An acid leached powder (6 N HCl, 6 N HNO_3, 3 h each at room temperature) and an unleached garnet fraction from this rock yield a three-point Sm–Nd whole-rock garnet isochron age of 320 ± 14 Ma (Fig. 4).

Zircon texture and geochronology

All migmatites contain multi-faceted, large euhedral zircon crystals (200–400 μm) with internal textures that appear to be very complex. Sample Ti1, leucocratic hornblende gneiss, contains elongate prismatic and equant zircon crystals of brownish colour. The grain interiors exhibit very low CL intensity and either are completely homogenous or

display very chaotic textures (Fig. 5a). These features are typical of zircons from granulite-facies rocks (Corfu et al. 2003). But we note that certain grains have high U and Th content (see below) and radiation damage by their decay may also suppress the CL emission (Geisler and Pidgeon 2001). The dark CL cores are surrounded by high-luminescent rims, and these rims may represent new zircon growth during a late high-temperature metamorphism (Fig. 5a). Four zircon crystals from sample Ti1 give $^{207}Pb/^{206}Pb$ evaporation ages between 336.8 ± 2.5 and 327.6 ± 3.2 Ma with a weighted mean age of 333.9 ± 4.4 Ma (Fig. 6a; Table 3). U–Pb SHRIMP data from the low-luminescent inner regions are apparently older (two spots at 341.1 ± 3.5 and 334.2 ± 3.4 Ma) compared with those of the bright luminescence outer zones (four spots between 325 and 320 Ma) (Figs. 7, 8a; Table 4).

Sample Hu1, mafic hornblende tonalitic gneiss, contains a zircon population composed of large transparent to translucent, long-prismatic crystals, frequently with inclusions of dark-coloured mineral phases and growth disconformities, but without evidence for oscillatory growth zoning or inherited cores. The zircons display either uniform CL or fluctuation between high- and low-luminescent domains (Figs. 5b, 7). The U–Pb isotope systematic of four single zircons from sample Hu1 was measured by ID-TIMS analyses (Table 5). These fractions, which were submitted to a thermal annealing experiment at 1,000 °C for 48 h (Mattinson 2005), plot along or near the concordia curve in the age range between 342 and 329 Ma (Fig. 6b). Regression of the data points, anchored at the origin, would yield an intercept age of 336.1 ± 7.8 Ma. Eleven U–Pb SHRIMP ages from high and low luminosity zones show no significant difference in $^{206}Pb/^{238}U$ age and all ages cluster between 331 and 320 Ma (Figs. 7, 8b; Table 4).

Wa1b is migmatitic gneiss with the best preserved granulite-facies assemblage among our samples (Fig. 2d). Zircons from sample Wa1b consist of translucent, white and brownish grains of short- or long-prismatic habits. CL images often reveal core-rim features with oscillatory zoned cores surrounded by recrystallized or newly grown rims (Figs. 5c, 7). Four zircon crystals from this sample give $^{207}Pb/^{206}Pb$ evaporation ages between 336.9 ± 2.6 and 331.1 ± 2.7 Ma with a weighted mean age of 333.5 ± 2.8 Ma (Fig. 6a; Table 3). Another four fractions from this sample were measured by ID-TIMS analyses (Table 5) and cluster along or near the concordia curve in the age range

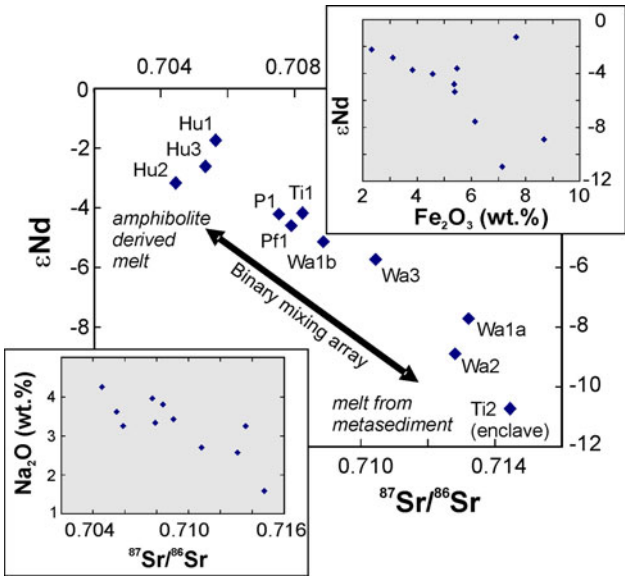

Fig. 3 Initial εNd versus initial $^{87}Sr/^{86}Sr$ isotope plot of samples from the migmatite complex. Sample Ti2 is from a granulite enclave. P1 and Pf1 (palite) taken from Siebel et al. (2005a, b). Insets: Na_2O versus $^{87}Sr/^{86}Sr$ and Fe_2O_3 versus εNd diagrams. $^{87}Sr/^{86}Sr$ and εNd values are those for 340 Ma

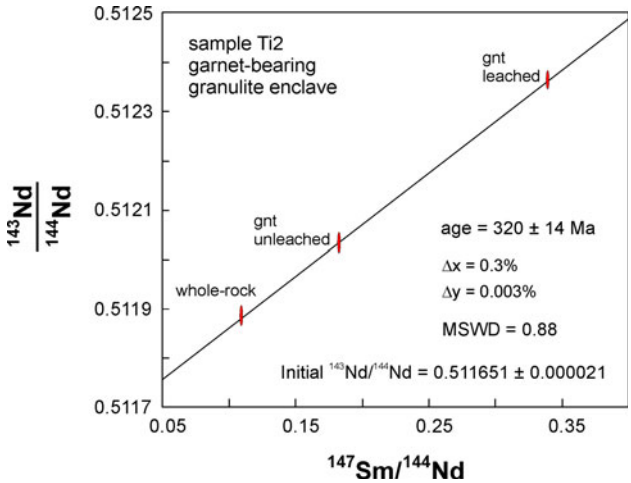

Fig. 4 Isochron plot presenting the results from garnet (leached and unleached fraction) + whole-rock Sm–Nd analyses of a granulite-facies enclave (sample Ti2). Quoted errors are 2σ

Table 2 Sm–Nd isotopic composition of two garnet fractions from granulite enclave sample Ti2

Sample Ti2	Sm (ppm)	Nd (ppm)	$^{147}Sm/^{144}Nd$	$^{143}Nd/^{144}Nd$	$\pm 2\sigma_{measured}$
Garnet unleached	5.22	17.29	0.1827	0.512028	0.000008
Garnet leached	2.84	5.07	0.3395	0.512364	0.000006

For whole-rock isotope data, see Table 1

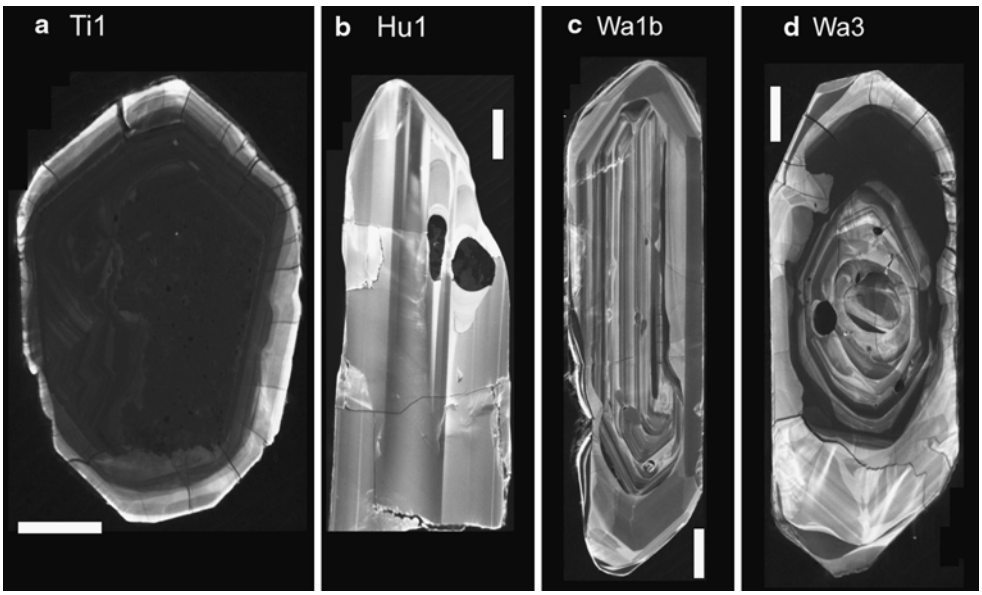

Fig. 5 Cathodoluminescence (CL) images of representative internal textures of zircons from the Bavarian migmatite complex. Length of scale *bars* = 50 μm. See text for details

between 341 and 320 Ma (Fig. 6b). Regression of these data points, anchored at the origin, would yield an intercept age of 335.5 ± 3.0 Ma. SHRIMP results reveal older $^{206}Pb/^{238}U$ ages for the low-luminescent inner domains (342–330 Ma) and younger rim ages between 334 and 327 Ma (Figs. 7, 8c; Table 4). The results also reveal $^{206}Pb/^{238}U$ ages of 375.0 ± 3.9, 420.3 ± 4.4 and 426.2 ± 4.4 Ma for three small core domains. This is the only evidence we found for the existence of pre-metamorphic xenocrystic cores.

Sample Wa3 is diatectic migmatite with abundant green hornblende (probably after pyroxene). The sample was collected from the Richardsreut quarry. As for sample Wa1b, the zircons display a diversity of recrystallization and replacement textures and new growth. Generally, inner domains of dark luminescence are surrounded by rims of bright luminescence with sector zoning in both domains (Figs. 5d, 7). In some grains, the rim zones display faint oscillatory zonation (Fig. 7). Zircons from sample Wa3 contain up to 2,000 ppm U and 700 ppm Th (Table 4), suggesting that some of the core areas with low CL response might be metamict (cf. Geisler and Pidgeon 2001). $^{207}Pb/^{206}Pb$ evaporation ages of six grains vary between 341.6 ± 3.6 and 330.5 ± 3.5 Ma with a weighted mean age of 336.4 ± 4.1 Ma (Fig. 6a; Table 2). $^{206}Pb/^{238}U$ SHRIMP ages obtained for the inner low-luminescent domains are older (generally between 341 and 320 Ma) whereas the high-luminescent rim zones yield younger ages between 333 and 320 Ma (Figs. 7, 8d; Table 4).

Discussion

Before we assess the implication of our results on zircon geochronology, we would like to point out an interesting aspect unveiled by whole-rock major element and isotopic data. It was already mentioned by Propach et al. (2008) and Finger et al. (2010) that the geochemical and isotopic diversity of the orthoanatexite unit and numerous mafic microgranular enclaves hosted in these rocks can be attributed to mingling and mixing of mafic and felsic melts. The wide range of Sr–Nd isotopic compositions (Table 1) is indicative of an isotopically heterogeneous magma body. In combination with major element data, these results allow further refinement on the compositional properties of end-member magmas involved in the mixing process. Surprisingly, the isotopically less-evolved members of the orthoanatexites ($^{87}Sr/^{86}Sr < 0.709$, $\varepsilon Nd > -5$) exhibit higher Na_2O and lower Fe_2O_3 contents than those observed in the isotopically evolved samples (Fig. 3). These observational constraints cannot be attributed to simple mantle–crust mixing. More likely, it reflects incomplete mixing between a sodium-rich trondhjemitic-tonalitic liquid, generated by partial melting of amphibolite/eclogite, and a melt derived from a metasedimentary source with isotopic characteristics of the granulite enclave. A very essential conclusion from these findings is that the orthoanatexite precursors formed by melting of crustal sources including amphibolites and pre-existing metasediments.

In terms of its geotectonic position, the orthogneiss unit from the southern Bavarian Forest was regarded as a relic

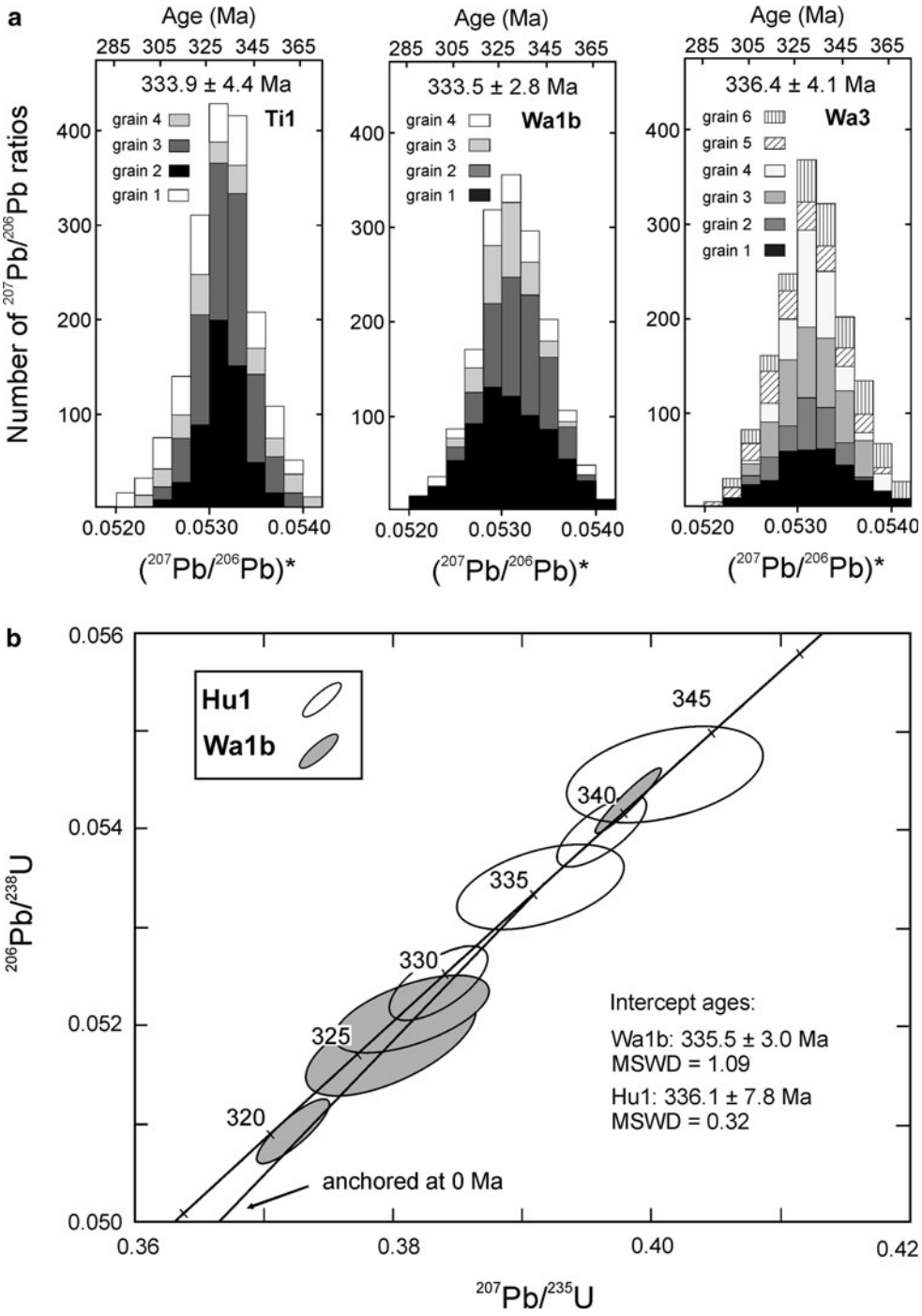

Fig. 6 **a** *Histograms* showing the distribution of radiogenic $^{207}Pb/^{206}Pb$ ratios obtained from Pb evaporation of single zircon grains from migmatite samples Ti1, Wa1b and Wa3; **b** U–Pb concordia diagrams of zircon analyses from samples Hu1 and Wa1b. Sample Hu1 thermally abraded, sample Wa1b non-abraded before U–Pb analyses. Individual analyses shown as 2σ *error ellipses*

of a Paleozoic volcanic island arc sequence (Propach et al. 2008). Finger et al. (2010) interpreted the rocks as a granodiorite intrusion that emplaced around 344 ± 2 Ma and later experienced intense high-temperature low-pressure regional anatectic conditions. These authors correlated the unit with the plutons of the Central Bohemian Batholith (Holub et al. 1997). Such model scenario critically depends on correct interpretation of the significance of measured ages. The results of zircon dating suggest the existence of a complex zircon population in the Bavarian orthogneiss complex. The following discussion therefore mainly focuses on the significance of these zircon ages.

The migmatite complex was subjected to severe polyphase Variscan deformation, and it is obvious from the zircon dates that the U–Pb isotopic systematics was disturbed by these processes. From the evidence provided by SHRIMP results, it becomes clear that the $^{207}Pb/^{206}Pb$ evaporation age data and the range of TIMS dates (i.e.

Table 3 $^{207}Pb/^{206}Pb$ evaporation data for single zircons from the migmatite complex

Sample/grain no.	No[a]	$^{204}Pb/^{206}Pb$	$^{208}Pb/^{206}Pb$	Th/U[b]	$^{207}Pb/^{206}Pb$[c]	Age (Ma)	Error (Ma)[d]
Ti1							
1	337	0.000742	0.05	0.17	0.052972 ± 50	327.6	3.2
2	524	0.000121	0.08	0.24	0.053148 ± 18	335.2	2.4
3	667	0.000356	0.07	0.21	0.053186 ± 22	336.8	2.5
4	228	0.000886	0.04	0.12	0.053164 ± 77	335.8	4.0
Weighted average						333.9	4.4
Wa1b							
1	719	0.000122	0.08	0.24	0.053092 ± 32	332.7	2.7
2	486	0.000032	0.06	0.20	0.053188 ± 26	336.9	2.6
3	254	0.000016	0.19	0.59	0.053054 ± 31	331.1	2.7
4	181	0.000028	0.14	0.43	0.053097 ± 58	333.0	3.4
Weighted average						333.5	2.8
Wa3							
1	317	0.000281	0.05	0.18	0.053176 ± 43	336.4	3.1
2	179	0.000029	0.06	0.20	0.053097 ± 43	333.5	3.0
3	358	0.000025	0.08	0.27	0.053199 ± 38	337.3	2.8
4	361	0.000029	0.06	0.19	0.053251 ± 30	339.5	2.6
5	212	0.000060	0.08	0.26	0.053039 ± 63	330.5	3.5
6	223	0.000228	0.03	0.12	0.053298 ± 65	341.6	3.6
Weighted average						336.4	4.1

[a] Number of measured $^{207}Pb/^{206}Pb$ isotope ratios per grain

[b] Model ratio calculated from radiogenic $^{208}Pb/^{206}Pb$ ratio and $^{207}Pb/^{206}Pb$ age of the sample

[c] $\pm 2\sigma$ standard deviation

[d] Error calculated using following formulae: $\sqrt{(2\sigma/\sqrt{n})^2+\Delta f^2}$, where n is the number of measured $^{207}Pb/^{206}Pb$ isotope ratios, 2σ is the 2-sigma standard error of the Gaussian frequency distribution function and Δf is an assumed uncertainty of the measured $^{207}Pb/^{206}Pb$ ratio of 0.1 %

single-grain dates) are produced by mixing of various amounts of older inner zone domains (i.e. those without relict cores) and younger rim domains with slightly different ages (i.e. ~340 vs. ~325 Ma). The same explanation may be applied for two previously investigated samples from the palites (Siebel et al. 2005a, b), which yield average $^{207}Pb/^{206}Pb$ evaporation zircon ages of 334 ± 3 Ma ($n = 5$) and 334.5 ± 1.1 Ma ($n = 6$), and $^{206}Pb/^{238}U$ TIMS ages between 342 and 327 Ma.

Evidently, the rocks were affected by two metamorphic events, an earlier high-pressure granulite-facies event, as indicated by the mineral paragenesis of sample Wa1b, and the late-Variscan metamorphic event (Bavarian phase), which reached anatectic pressure–temperature conditions. The age of granulite-facies metamorphism in the Bavarian Forest has not yet been well determined. Zircon rims in adjacent garnet-biotite and biotite-plagioclase gneisses of the Kropfmühl series are interpreted to have grown during this high-grade metamorphic stage at ~340 Ma (Teipel et al. 2002). The Sm–Nd garnet age of the granulite enclaves (320 ± 14 Ma), although not rigorous, arguably reflects a high-grade metamorphic event. Granulite-facies metamorphism is better constrained in the southwest Bohemian Massif by zircon ages around 340–345 Ma (Kröner et al. 2000; Wendt et al. 1994). In the light of this evidence, two different tectonothermal evolution models for the orthogneiss complex are conceivable:

1. The zircon ages of ~340 Ma obtained from inner zone domains date the intrusion of the orthogneiss progenitor, and all younger ages are related to complex metamorphic overprint. According to this concept, favoured by Finger et al. (2010), the protolith was generated in a Lower Carboniferous continental margin or island arc tectonic setting, and the oldest $^{206}Pb/^{238}U$ ages (~420 Ma, this study, ~580 Ma Finger et al. 2010) represent pre-magmatic inherited cores.
2. The igneous protolith of the orthogneisses is older than most of the zircon ages. From geological relationships, an Early Palaeozoic age of the complex is a reasonable estimate (Propach et al. 2008). In this scenario, the zircon ages of ~340 Ma and 330–320 Ma approximate the time of two high-grade metamorphic events that affected the gneiss complex during the Carboniferous.

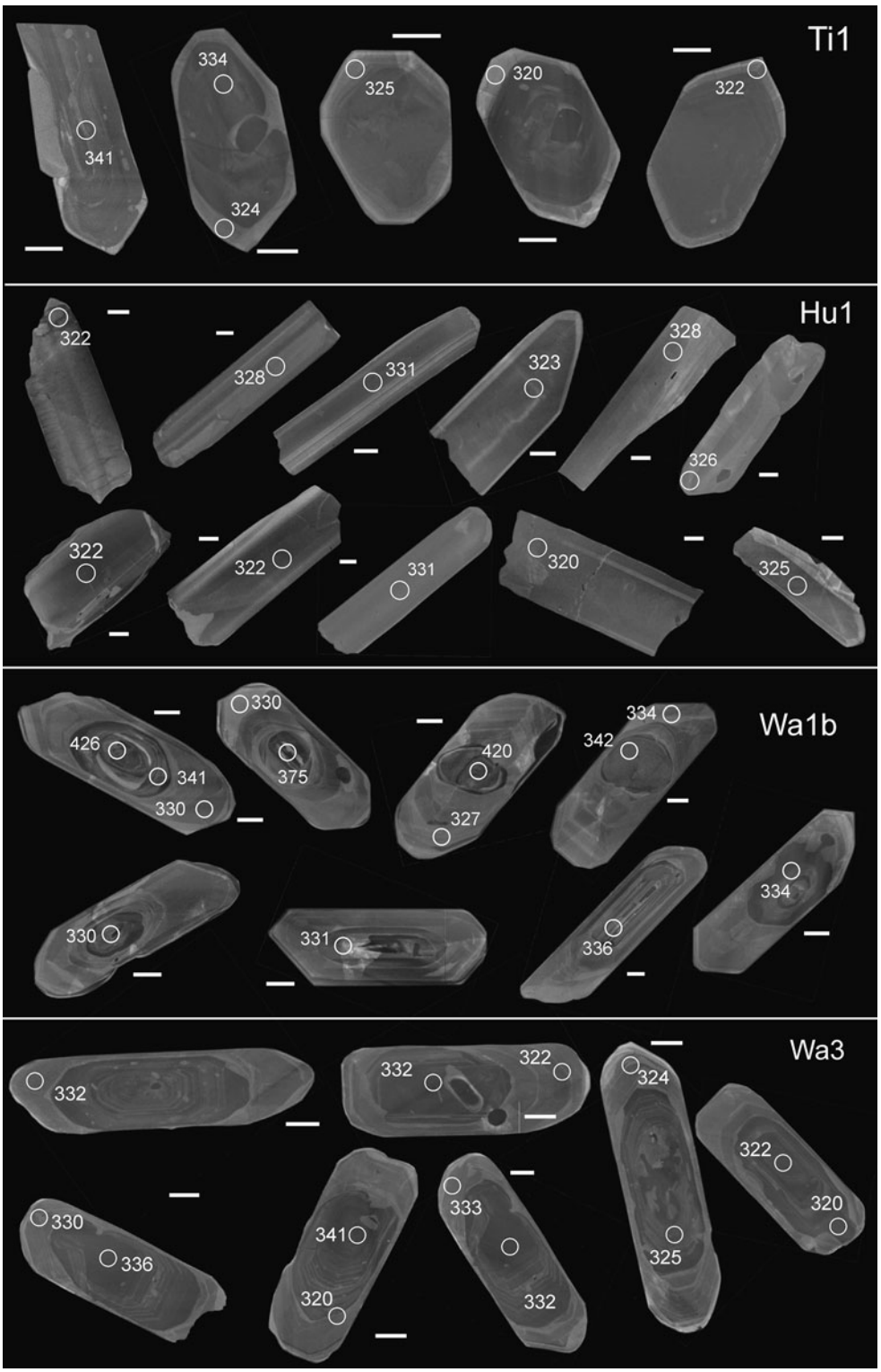

Fig. 7 Cathodoluminescence images of zircons from SHRIMP dated samples of the migmatite complex. Length of scale *bars* = 50 μm. Analytical spots and obtained $^{206}Pb/^{238}U$ ages (in Ma) are shown. Most zircon crystals contain distinct interiors and rims and a systematic trend of younger ages in zircon rims (high-luminescent domains) can be observed

The crystallization time of the migmatite precursor is not easy to reconcile with the U–Pb analytical data. Since there is no unambiguous proof that the three $^{206}Pb/^{238}U$ SHRIMP ages obtained from inner cores of Wa1b (375.0 ± 3.9, 420.3 ± 4.4 and 426.2 ± 4.4 Ma) represent the relict from original igneous zircon, the possibility of a

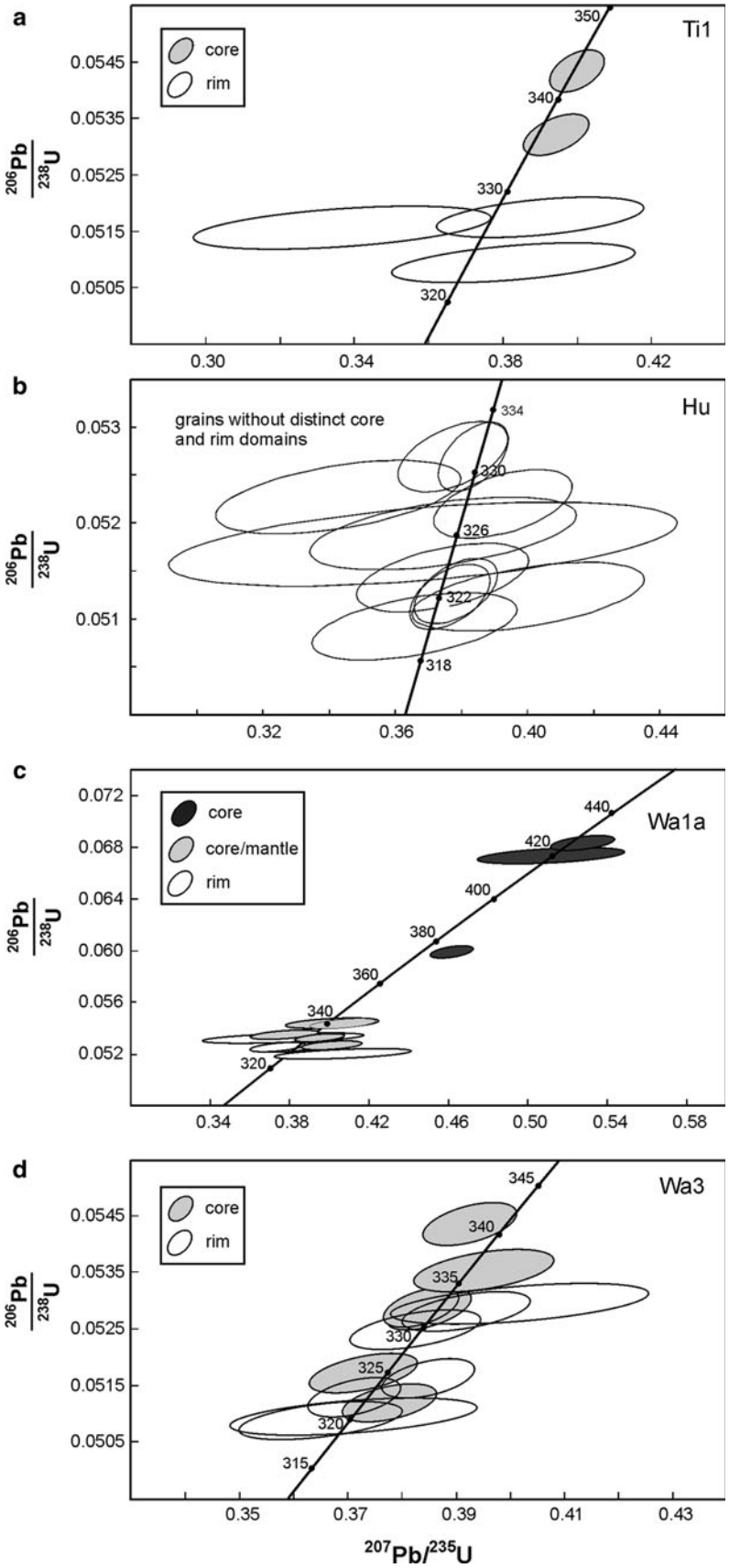

Fig. 8 Wetherill concordia plots of SHRIMP U/Pb zircon data of samples **a** Ti1, **b** Hu1, **c** Wa1b and **d** Wa3. Individual analyses are shown as two sigma *error ellipses*. *Dark grey error ellipses* inherited zircon cores from sample Wa1a. *Light grey error ellipses* metamorphic grown inner zone domains without inherited cores; *white error ellipses* metamorphic grown rims or grains without distinct core and rim domains (sample Hu1)

Table 4 U–Th–Pb shrimp analytical data for zircons from the migmatite complex

Grain.spot	U ppm	Th ppm	Th/U	Pb ppm	$^{207}Pb/^{206}Pb$ 204corr	±1σ %	$^{206}Pb/^{238}U$ 204corr	±1σ %
TI1-1.1[a]	1,335	27	0.02	65	0.0537	0.95	0.05321	1.053
TI1-3.1[a]	1,258	838	0.67	74	0.0534	0.56	0.05435	1.051
TI1-5.1	181	181	1.00	11	0.0545	5.91	0.05096	1.119
TI1-4.1	865	116	0.13	43	0.0551	2.25	0.05122	1.060
TI1-1.2	1,043	107	0.10	86	0.0474	9.47	0.05157	1.148
TI1-2.1	391	197	0.50	21	0.0547	4.69	0.05175	1.088
HU1-9.1	392	556	1.42	26	0.0521	6.08	0.05092	1.106
HU1-11.1	350	641	1.83	25	0.0533	1.96	0.05123	1.060
HU1-4.1	202	206	1.02	12	0.0566	5.74	0.05123	1.114
HU1-6.1	474	871	1.84	34	0.0535	1.99	0.05129	1.061
HU1-3.1	153	166	1.08	9	0.0528	4.78	0.05143	1.101
HU1-10.1	278	370	1.33	18	0.0516	15.19	0.05178	1.336
HU1-8.1	118	110	0.93	7	0.0523	7.61	0.05189	1.152
HU1-7.1	287	420	1.46	19	0.0545	3.40	0.05220	1.075
HU1-5.1	131	164	1.25	9	0.0476	8.35	0.05227	1.146
HU1-2.1	149	188	1.26	10	0.0520	2.85	0.05269	1.078
HU1-1.1	360	591	1.64	26	0.0528	1.52	0.05269	1.059
WA3-7.1[a]	551	44	0.08	26	0.0535	1.19	0.05119	1.055
WA3-4.1[a]	1,136	308	0.27	59	0.0523	1.53	0.05171	1.054
WA3-3.1[a]	2,065	744	0.36	110	0.0528	0.85	0.05284	1.052
WA3-5.1[a]	1,575	634	0.40	84	0.0526	0.62	0.05287	1.052
WA3-2.1[a]	597	123	0.21	31	0.0535	1.88	0.05353	1.057
WA3-6.1[a]	2,324	665	0.29	126	0.0524	1.00	0.05436	1.052
WA3-7.2	422	161	0.38	22	0.0520	2.74	0.05088	1.065
WA3-6.2	393	158	0.40	20	0.0528	4.26	0.05095	1.082
WA3-5.2	398	160	0.40	21	0.0525	1.21	0.05128	1.057
WA3-4.2	354	140	0.40	19	0.0541	1.06	0.05162	1.056
WA3-2.2	432	185	0.43	23	0.0528	1.84	0.05248	1.059
WA3-1.2	434	183	0.42	23	0.0538	1.67	0.05280	1.057
WA3-3.2	379	156	0.41	20	0.0550	3.77	0.05294	1.077
WA1B-2.1[b]	532	363	0.68	35	0.0559	0.76	0.05989	1.057
WA1B-8.1[b]	413	184	0.45	29	0.0551	3.61	0.06737	1.079
WA1B-1.1[b]	481	110	0.23	32	0.0560	1.02	0.06835	1.058
WA1B-6.1[a]	477	192	0.40	25	0.0532	2.97	0.05248	1.067
WA1B-4.2[a]	327	319	0.97	20	0.0553	2.26	0.05266	1.063
WA1B-5.1[a]	602	104	0.17	31	0.0539	1.76	0.05322	1.058
WA1B-7.1[a]	350	55	0.16	18	0.0512	3.00	0.05349	1.067
WA1B-1.3[a]	364	19	0.05	18	0.0543	2.45	0.05435	1.063
WA1B-3.1[a]	328	14	0.04	16	0.0535	3.68	0.05442	1.075
WA1B-8.2	181	120	0.66	10	0.0568	5.39	0.05199	1.108
WA1B-1.2	307	265	0.86	18	0.0517	2.40	0.05249	1.065
WA1B-2.2	144	74	0.51	8	0.0530	1.59	0.05252	1.066
WA1B-3.2	194	120	0.62	11	0.0514	7.66	0.05321	1.137

Grain.spot	$^{207}Pb/^{235}U$ 204corr	±1σ %	%c	$^{206}Pb/^{238}U$ date (Ma)	±1σ Ma	$^{207}Pb/^{235}U$ date (Ma)	±1σ Ma
TI1-1.1[a]	0.3943	1.51	93	334.2	3.4	337.5	4.3
TI1-3.1[a]	0.4001	1.25	99	341.2	3.5	341.7	3.6
TI1-5.1	0.3826	6.15	82	320.4	3.5	329.0	17.3
TI1-4.1	0.3888	2.60	78	322.0	3.3	333.5	7.4

Table 4 continued

Grain.spot	$^{207}Pb/^{235}U$ 204corr	$\pm1\sigma$ %	%c	$^{206}Pb/^{238}U$ date (Ma)	$\pm1\sigma$ Ma	$^{207}Pb/^{235}U$ date (Ma)	$\pm1\sigma$ Ma
TI1-1.2	0.3369	9.68	472	324.2	3.6	294.9	24.8
TI1-2.1	0.3901	4.94	82	325.3	3.5	334.4	14.1
HU1-9.1	0.3658	6.32	110	320.1	3.5	316.6	17.2
HU1-11.1	0.3765	2.34	94	322.1	3.3	324.5	6.5
HU1-4.1	0.4001	5.98	67	322.1	3.5	341.8	17.4
HU1-6.1	0.3783	2.37	92	322.5	3.3	325.8	6.6
HU1-3.1	0.3743	5.04	101	323.3	3.5	322.8	13.9
HU1-10.1	0.3684	15.42	122	325.5	4.2	318.5	42.2
HU1-8.1	0.3745	7.84	109	326.1	3.7	323.0	21.7
HU1-7.1	0.3926	3.70	83	328.0	3.4	336.2	10.6
HU1-5.1	0.3429	8.57	421	328.5	3.7	299.4	22.2
HU1-2.1	0.3774	3.17	117	331.0	3.5	325.1	8.8
HU1-1.1	0.3836	1.96	103	331.0	3.4	329.7	5.5
WA3-7.1[a]	0.3777	1.69	92	321.8	3.3	325.3	4.7
WA3-4.1[a]	0.3730	1.96	109	325.0	3.3	321.9	5.4
WA3-3.1[a]	0.3849	1.44	103	331.9	3.4	330.6	4.1
WA3-5.1[a]	0.3835	1.28	106	332.1	3.4	329.6	3.6
WA3-2.1[a]	0.3951	2.27	96	336.1	3.5	338.1	6.5
WA3-6.1[a]	0.3924	1.54	113	341.2	3.5	336.1	4.4
WA3-7.2	0.3650	3.06	112	319.9	3.3	316.0	8.3
WA3-6.2	0.3711	4.53	100	320.4	3.4	320.5	12.4
WA3-5.2	0.3712	1.70	105	322.4	3.3	320.5	4.7
WA3-4.2	0.3848	1.58	87	324.5	3.3	330.5	4.5
WA3-2.2	0.3824	2.24	102	329.7	3.4	328.8	6.3
WA3-1.2	0.3919	2.09	91	331.7	3.4	335.8	6.0
WA3-3.2	0.4017	4.04	80	332.6	3.5	342.9	11.8
WA1B-2.1[b]	0.4617	1.38	84	375.0	3.9	385.5	4.4
WA1B-8.1[b]	0.5121	3.90	101	420.3	4.4	419.9	13.4
WA1B-1.1[b]	0.5274	1.56	95	426.2	4.4	430.1	5.5
WA1B-6.1[a]	0.3848	3.28	98	329.8	3.4	330.6	9.3
WA1B-4.2[a]	0.4012	2.62	78	330.8	3.4	342.6	7.6
WA1B-5.1[a]	0.3952	2.16	92	334.3	3.5	338.2	6.2
WA1B-7.1[a]	0.3773	3.30	136	335.9	3.5	325.1	9.2
WA1B-1.3[a]	0.4070	2.79	89	341.2	3.5	346.8	8.2
WA1B-3.1[a]	0.4012	3.96	98	341.6	3.6	342.5	11.5
WA1B-8.2	0.4069	5.63	68	326.7	3.5	346.6	16.5
WA1B-1.2	0.3740	2.74	122	329.8	3.4	322.6	7.6
WA1B-2.2	0.3839	2.03	100	330.0	3.4	329.9	5.7
WA1B-3.2	0.3768	7.89	130	334.2	3.7	324.7	21.9

207Pb/206Pb 204corr = 204Pb-corrected 207Pb/206Pb ratio

206Pb/238U 204corr = 204Pb-corrected 206Pb/238U ratio

207Pb/235U 204corr = 204Pb-corrected 207Pb/235U ratio

%c = % Concordance

206Pb/238U date = 204Pb-corrected 206Pb/238U date

207Pb/235U date = 204Pb-corrected 207Pb/235U date

207Pb/206Pb date = 204Pb-corrected 207Pb/206Pb date

[a] Inner zone domain without relict core;

[b] Relict core

Table 5 U-Pb ID-TIMS data for zircon fractions from the migmatite complex

Sample/ fraction	Weight[a] (mg)	$^{206}Pb^{b}/^{204}Pb$	U (ppm)	Pb (ppm)	$^{208}P/^{206}Pb$	Atomic ratios[c]			Apparent ages (Ma)		
						$^{206}Pb/^{238}U$	$^{207}Pb/^{235}U$	$^{207}Pb/^{206}Pb$	$^{206}P/^{238}U$	$^{207}P/^{235}U$	$^{207}Pb/^{206}Pb$
Hu1											
1[d]	0.078	8,006	209	14	0.38	0.05397 ± 30	0.3962 ± 29	0.05323 ± 26	339	339	339
2[d]	0.043	1,518	123	8.3	0.36	0.05455 ± 40	0.4011 ± 63	0.05332 ± 77	342	342	342
3[d]	0.045	4,306	277	19	0.44	0.05243 ± 31	0.3835 ± 32	0.05305 ± 32	329	330	331
4[d]	0.035	4,278	247	17	0.40	0.05342 ± 36	0.3915 ± 54	0.05315 ± 66	335	335	335
Wa1b											
1	0.060	5,020	302	16	0.17	0.05092 ± 27	0.3723 ± 23	0.05302 ± 17	320	321	330
2	0.027	3,925	484	26	0.08	0.05180 ± 44	0.3798 ± 54	0.05318 ± 59	326	327	336
3	0.024	2,890	389	23	0.18	0.05430 ± 28	0.3982 ± 22	0.05319 ± 10	341	340	337
4	0.014	2,137	284	16	0.17	0.05212 ± 32	0.3815 ± 50	0.05308 ± 58	328	328	332

All isotopic measurements corrected for instrumental mass bias of 1 ‰ per mass unit

[a] Weight and concentration error better than 20%

[b] Measured ratio corrected for mass discrimination and spike contribution

[c] Corrected for blank Pb, U, and initial Pb with $^{206}Pb/^{204}Pb = 18.24$, $^{207}Pb/^{204}Pb = 15.60$; errors are $2\sigma_m$

[d] Thermally abraded zircon fractions

xenocrystic origin cannot be completely ruled out. Indirect constraints on primary crystallization of the orthogneiss complex are provided by the study of similar rocks: a Devonian magmatic protolith age (~370 Ma, U–Pb zircon age) was assigned for granulites from southern Bohemia (Wendt et al. 1994), and orthogneisses from the Austrian part yielded Early Palaeozoic (Cadomian and Ordovician) protolith ages (Friedl et al. 2004; Kröner et al. 2000).

Based on textural information, two types of zircon domains can be distinguished in most of the migmatite samples: zones that are characterized by structureless low-intensity CL emission and those with usually bright luminescence and planar banded zoning (Fig. 5). Except sample Hu1 where CL emission contrasts are more randomly distributed within the crystals (Fig. 5b), darker central areas are generally concentrically overgrown by brighter rim zones (Fig. 5a, c, d). We consider that the low-luminescent zircon domains are the result of metamorphic transformation rather than new zircon growth. In CL images, this interpretation is supported by the lack of igneous growth textures, dark featureless zones and areas of sector zoning in the inner parts of the grains (Fig. 5). Similar characteristics are reported in a number of other studies on zircons from metamorphic rocks (e.g. Schaltegger et al. 1999; Vavra et al. 1999; Corfu et al. 2003). It was already noted that partial loss of radiogenic Pb associated with structural transformation processes can produce U–Pb dates that are younger than the zircon crystallization age (e.g. Hoskin and Black 2000). Th/U ratios from the low-intensity CL core zones are relatively high, on average 0.29 ($n = 14$, Ti1, Wa1b, Wa3, Table 4), and thus within the range of igneous zircon. High Th/U ratios, however, have been also reported from recrystallized zircons or zircons grown in high-temperature regimes (see Piedgeon 1992; Harley et al. 2007 and references therein). From these observations, we conclude that the U–Pb system of the inner zircon domains was reset to various extents during granulite-facies metamorphism. The upper age limit obtained from those domains (~340 Ma) would be the best estimate for the time of granulite metamorphic overprint of the orthogneisses. Overall, spots in the inner domains gave $^{206}Pb/^{238}U$ ages between 342 and 322 Ma with a weighted mean $^{238}U/^{206}Pb$ age of 333.6 ± 3.1 Ma. The fact that these domains suffered a second high-grade thermal event during the Bavarian metamorphic phase could be a reasonable explanation for the more pronounced age variability of the inner zone domains compared with the rims. An additional explanation for this age variation is that secondary radiation damage might have affected the U–Pb systematic of inner zircon domains. As mentioned above, the low CL intensity in inner domains of samples Ti1 and Wa3 might be the result of metamictization. Although the degree of metamictization was not constrained for the investigated zircons, such process would result in a weakening of the zircon structure. The large scatter of ages in the core zones from these grains (down to 320 Ma in sample Wa3) could thus reflect the effect of Pb loss from radiation damaged zircon domains.

According to the $^{238}U/^{206}Pb$ SHRIMP ages, the rim zones represent zircon growth domains developed during the final metamorphic stage. The weighted mean $^{238}U/^{206}Pb$ age of 326.0 ± 2.8 Ma obtained for fourteen

zircon rim domains corresponds with the U–Pb ages of 326–323 Ma reported for the late-Variscan thermal overprint (Kalt et al. 2000). Th/U ratios are higher in the rim zones (0.48, $n = 15$, samples Ti1, Wa1b, Wa3, Table 4) than in the grain centres (0.29, $n = 14$), but are characterized by significantly lower trace element contents: U = 409 ppm, Th = 155 ppm, Pb = 24 ppm in rims compared with U = 949 ppm, Th = 292 ppm and Pb = 50 ppm in inner zone domains. Such relation is strongly analogous to zircon grains affected by metamorphic re-equilibration (Geisler et al. 2007 and references therein). In such case, earlier crystallized U–Th-rich zones are replaced by late U–Th-poor zircon. This modification is attributed to the reaction of zircon with a melt fraction, and there was certainly a melt phase present in the rocks during late-Variscan anatexis. Growth of zircon in the presence of melt would also explain the general lack of distinctive round anhedral zircon morphologies usually found in metamorphic rocks, which formed below melting temperatures (Corfu et al. 2003).

Zircon saturation temperatures (Watson and Harrison 1983) calculated from bulk rock compositions of ten migmatite samples (Table 1) range from 782 to 890 °C (mean = 831 °C). If the melt produced during metamorphic melting was undersaturated in zirconium, as indicated by the general lack of zircon inheritance, these temperatures should be the minimum temperature that prevailed during crystal growth. However, since the textures of these rocks provide strong evidence for polymetamorphism involving dehydration reactions and thus multiple melt loss or gain events, it is difficult to decide what whole-rock composition was saturated with respect to Zr during which phase of zircon growth, and thus, caution is warranted about interpreting the significance of these temperatures despite the absence of zircon inheritance.

Although studies on the kinetics of zircon dissolution in crustal melts are rare, some studies have provided evidence for the re-equilibration of natural zircon in a melt phase (see Geisler et al. 2007; Gagnevin et al. 2010). Dissolution behaviour depends on several factors such as zircon size, volume, alkalinity and temperature of the melt reservoir with which the zircons interact (Watson and Harrison 1983). For zircons from south Bohemian granulites, it was argued that during post-peak granulite-facies metamorphism and formation of a melt phase, pre-existing grains were dissolved in the melt and new zircons crystallized (Roberts and Finger 1997). In this example, peak metamorphic temperatures of 900–1,050 °C were attained (Carswell and O'Brian 1993). Nevertheless, felsic granulites from southern Bohemia contain inherited old zircons (Roberts and Finger 1997; Wendt et al. 1994). In the present study, only one sample (Wa1b) provides some evidence for pre-metamorphic zircon growth. This leads to the conclusion that granulite metamorphism has strongly erased initial (inherited or primary magmatic) zircon. The scarcity of older inherited cores and the lack of small zircon crystals in the rocks could be a result of dissolution of smaller crystals in a melt. Dissolution of zircon would increase zircon saturation of the melt and promote formation of overgrowth on larger grains via Ostwald ripening (Nemchin et al. 2001). Overall, the range of zircon ages that has been found (i.e. 342–320 Ma) could reflect a protracted period of zircon transformation, followed by dissolution and growth of new rims around transformed grains during decompression melting from granulite (i.e. 345–340 Ma) to amphibolite-facies conditions (326–323 Ma). Such interpretation is substantiated by recent studies showing that zircons from high-grade rocks do not necessarily date peak metamorphic conditions, but can re-equilibrate and grow during retrograde stages (Hermann et al. 2006; Whitehouse and Platt 2003).

Conclusions

A large region of the southern Bavarian Forest is composed of anatectic rocks comprising migmatites/orthoanatexites, with subordinate paragneiss enclaves and relict domains having granulite affinities. Field relations and geochemical and isotopic composition of this unit favours magma mixing between a trondhjemitic-tonalitic progenitor and anatectic material derived from supracrustal rocks. Our study reveals complex internal zircon textures and age information for the migmatites. The observed range of zircon ages prevents us from placing tight constraints on primary crystallization of the gneiss protolith from an igneous melt. Most likely, originally magmatic zircons were overprinted between two high-grade metamorphic events between ~340 Ma and 326–323 Ma. The older metamorphic event is related to granulite-facies metamorphism whereas the younger event was associated with the late-Variscan anatexis. We conclude that the migmatites from the Bavarian Forest have undergone pervasive dehydration melting of biotite and probably amphibole, during and after granulite-facies metamorphism and during regional decompression and exhumation. These processes first resulted in rejuvenation of pre-existing zircon grains followed by dissolution and growth of new zircon domains.

Acknowledgments S. Eroglu, A. Frew, E. Kiemele and E. Reitter are thanked for help during isotope analyses. We are grateful to G. Markl, M. Marks, G. Propach and T. Wenzel for support and fruitful discussions and to F. Corfu, F. Finger, Th. Geisler-Wierwille, K. Mezger, I. Williams and two anonymous reviewers for critical comments. This research has been benefitted from financial support of the Bayerische Landesamt für Umwelt.

References

Carswell DA, O'Brian PJ (1993) Thermobarometry and geotectonic significance of high-pressure granulites—examples from the Moldanubian zone of the Bohemian Massif in Lower Austria. J Petrol 34:427–459

Compston W, Williams IS, Meyer C (1984) U-Pb geochronology of zircons from lunar breccia 73,217 using a sensitive high mass-resolution ion microprobe. J Geophys Res 89:B252–B534

Connelly JN (2001) Constraining the timing of metamorphism: U–Pb and Sm–Nd ages from a transect across the Northern Torngat orogen, Labrador, Canada. J Geol 109:57–77

Corfu F, Hanchar JM, Hoskin PWO, Kinny P (2003) Atlas of zircon textures. In: Hanchar JM, Hoskin PWO (eds) Rev Mineral Geochem. Mineral Soc Am 53:469–500

Crock JG, Lichte FE, Wildeman TR (1984) The group separation of the rare-earth elements and yttrium from geologic materials by cation-exchange chromatography. Chem Geol 45:149–163

Crowley JL, Brown RL, Gervais F, Gibson HD (2008) Assessing inheritance of zircon and monazite in granitic rocks from the Monashee complex, Canadian Cordillera. J Petrol 49:1915–1929

Cumming GL, Richards JR (1975) Ore lead isotope ratios in a continuously changing earth. Earth Planet Sci Lett 28:155–171

Fiala J, Fuchs G, Wendt JI (1995) Stratigraphy of the Moldanubian zone. In: Dallmeyer RD, Franke W, Weber K (eds) Pre-permian geology of central and eastern Europe. Springer, Berlin, pp 417–428

Finger F, Gerdes A, Janoušek V, René M, Riegler G (2007) Resolving the Variscan evolution of the Moldanubian sector of the Bohemian Massif: the significance of the Bavarian and the Moravo-Moldanubian tectonometamorphic phases. J Geosci 52:9–28

Finger F, Dunkley DJ, René M (2010) Remnants of early Carboniferous I-type granodiorite plutons in the Bavarian Forest and their bearing on the tectonic interpretation of the south-western sector of the Bohemian Massif (Bavarian zone). J Geosci 55:321–332

Franke W (2000) The mid-European segment of the Variscides: tectonostratigraphic units, terrane boundaries and plate tectonic evolution. In: Franke W, Haak V, Oncken O, Tanner D (eds) Orogenic processes: quantification and modelling in the Variscan belt. Spec Publ Geol Soc, London, vol 179, pp 35–61

Frentzel A (1911) Das Passauer Granitmassiv. Geognostisches Jahrb 24:31

Friedl G, Finger F, Paquette JL, von Quadt A, Mcnaughton NJ, Fletcher IR (2004) Pre-Variscan geological events in the Austrian part of the Bohemian Massif deduced from U–Pb zircon ages. Int J Earth Sci 93:802–823

Gagnevin D, Daly JS, Kronz A (2010) Zircon texture and chemical composition as a guide to magmatic processes and mixing in a granitic environment and coeval volcanic system. Contrib Miner Petrol 159:579–596

Gebauer D, Williams IS, Compston W, Grünenfelder M (1989) The development of the Central European continental-crust since the early Archean based on conventional and ion-microprobe dating of up to 3.84 b.y. old detrital zircons. Tectonophysics 157:81–96

Geisler T, Pidgeon RT (2001) Significance of radiation damage on the integral SEM cathodoluminescence intensity of zircon: an experimental annealing study. N Jb Miner Mh 10:433–445

Geisler T, Schaltegger U, Tomaschek F (2007) Re-equilibration of zircon in aqueous fluids and melts. Elements 3:43–50

Goldstein SL, O'Nions RK, Hamilton PJ (1984) A Sm–Nd study of atmospheric dusts and particulates from major river systems. Earth Planet Sci Lett 70:221–236

Grant ML, Wilde SA, Wu FY, Yang JH (2009) The application of zircon cathodoluminescence imaging, Th–U–Pb chemistry and U–Pb ages in interpreting discrete magmatic and high-grade metamorphic events in the North China Craton at the Archean/Proterozoic boundary. Chem Geol 261:154–170

Guo JH, Sun M, Chen FK, Zhai MG (2005) Sm–Nd and SHRIMP U–Pb zircon geochronology of high-pressure granulites in the Sanggan area, North China craton: timing of Paleoproterozoic continental collision. J Asian Earth Sci 24:629–642

Harley SL, Kelly NM, Möller A (2007) Zircon behaviour and the thermal histories of mountain chains. Elements 3:25–30

Hermann J, Rubatto A, Rommsdorff V (2006) Sub-solidus Oligocene zircon formation in garnet peridotite during fast decompression and fluid infiltration (Duria, Central Alps). Miner Petrol 88:181–206

Holub FV, Machart J, Manová M (1997) The Central Bohemian plutonic complex: geology, chemical composition and genetic interpretation. J Geol Sci Econ Geol Miner 31:27–51

Hoskin PWO, Black LP (2000) Metamorphic zircon formation by solid state recrystallization of protolith igneoud zircon. J Metamorph Geol 18:423–439

Humphreys HC, Cornell DH (1989) Petrology and geochronology of low-pressure mafic granulites in the Marydale group, South Africa. Lithos 22:287–303

Jacobsen K, Wasserburg GJ (1980) Sm–Nd isotopic evolution of chondrites. Earth Planet Sci Lett 50:139–155

Janoušek V, Vrána S, Erban V, Vokurka K, Drábek M (2008) Metabasic rocks in the Varied group of the Moldanubian zone, southern Bohemia—their petrology, geochemical character and possible petrogenesis. J Geosci 53:31–64

Kalt A, Corfu F, Wijbrans JR (2000) Time calibration of a P-T path from a Variscan high-temperature low-pressure metamorphic complex (Bayerische Wald, Germany), and the detection of inherited monazite. Contrib Miner Petrol 138:143–163

Klötzli US (1997) Single zircon evaporation thermal ionisation mass spectrometry: methods and procedures. Analyst 122:1239–1248

Kober B (1987) Single-zircon evaporation combined with Pb^+ emitter-bedding for $^{207}Pb/^{206}Pb$-age investigations using thermal ion mass spectrometry, and implications to zirconology. Contrib Miner Petrol 96:63–71

Kröner A, Wendt I, Liew TC, Compston W, Todt W, Fiala J, Vaňková V, Vaněk J (1988) U–Pb zircon and Sm–Nd model ages of high-grade Moldanubian metasediments, Bohemian Massif, Czechoslovakia. Contrib Miner Petrol 99:257–266

Kröner A, O'Brian PJ, Nemchin AA, Pidgeon RT (2000) Zircon ages for high pressure granulites from South Bohemia, Czech Republic, and their connection to Carboniferous high temperature processes. Contrib Miner Petrol 138:127–142

Liu YS, Gao S, Hu ZC, Gao CG, Zong K, Wang D (2010) Continental and oceanic crust recycling-induced melt-peridotite interactions in the Trans-North China Orogen: U–Pb dating, Hf isotopes and trace elements in zircons from mantle xenoliths. J Petrol 51:537–571

Ludwig KR (2003) Isoplot 3.0: a geochronological toolkit for Microsoft Excel Berkeley Geochronology Center, Spec Publ 4

Manhès G, Minster JF, Allègre CJ (1978) Comparative uranium-thorium-lead and rubidium-strontium study of the Saint Severin amphoterite: consequences for early solar system chronology. Earth Planet Sci Lett 39:14–24

Mattinson JM (2005) Zircon U–Pb chemical abrasion ("CA-TIMS") method: combined annealing and multi-step partial dissolution analysis for improved precision and accuracy of zircon ages. Chem Geol 220:47–66

Mezger K, Krogstad EJ (1997) Interpretation of discordant U–Pb zircon ages: an evaluation. J Metamorph Geol 15:127–140

Möller A, O'Brian PJ, Kennedy A, Kröner A (2002) Polyphase zircon in ultrahigh-temperature granulites (Rogaland, SW Norway):

constraints for Pb diffusion in zircon. J Metamorph Geol 20: 727–740

Nasdala L, Hofmeister W, Norberg N, Martinson JM, Corfu F, Dörr W, Kamo SL, Kennedy AK, Kronz A, Reiners PW, Frei D, Kosler J, Wan Y, Götze J, Häger T, Kröner A, Valley JW (2008) Zircon M257—a homogeneous natural reference material for the ion microprobe U–Pb analysis of zircon. Geostand Geoanal Res 32:247–265

Nelson DR (1997) Compilation of SHRIMP U–Pb zircon geochronology data, 1996. Geol Surv West Aust Rec 1997(2):189

Nelson DR (2001) Compilation of geochronology data, 2000. Geol Surv West Aust Rec 2001(2):205

Nelson DR (2006) CONCH: a visual basic program for interactive processing of ion-microprobe analytical data. Comput Geosci 32:1479–1498

Nemchin AA, Giannini LM, Bodorkos S, Oliver NHS (2001) Ostwald ripening as a possible mechanism for zircon overgrowth formation during anatexis: theoretical constraints, a numerical model, and its application to pelitic migmatites of the Tickalara metamorphics, northwestern Australia. Geochim Cosmochim Acta 65:2771–2788

Piedgeon RT (1992) Recrystallisation of oscillatory zoned zircon: some geochronological and petrological implications. Contrib Miner Petrol 110:463–472

Potts PJ, Webb PC (1992) X-ray-fluorescence spectrometry. J Geochem Explor 44:251–296

Propach G, Kling M, Lindhardt E, Rohrmüller J (2008) Remnants of an island arc within the Moldanubian zone of the Bavarian Forest. Geol Bavarica 110:343–377

Richard P, Schmizu N, Allègre CJ (1976) $^{143}Nd/^{144}Nd$, a natural tracer: an application to oceanic basalts. Earth Planet Sci Lett 31:269–278

Roberts MP, Finger F (1997) Do U–Pb zircon ages from granulites reflect peak metamorphic conditions? Geology 25:319–322

Rubatto D, Scambelluri M (2003) U–Pb dating of magmatic zircon and metamorphic baddeleyite in the Ligurian eclogites (Voltri Massif, Western Alps). Contrib Miner Petrol 146:341–355

Schaltegger U, Fanning CM, Gunther D, Maurin DC, Schulmann K, Gebauer D (1999) Growth, annealing and recrystallization of zircon and preservation of monazite in high-grade metamorphism: conventional and in situ U–Pb isotope, cathodoluminescence and microchemical evidence. Contrib Miner Petrol 134:186–201

Scherer EE, Whitehouse MJ, Münker C (2007) Zircon as a monitor of crustal growth. Elements 3:19–24

Schulmann K, Kröner A, Hegner E, Wendt JI, Konopásek J, Lexa O, Štipska P (2005) Chronological constraints on the pre-orogenic history, burial and exhumation of deep-seated rocks along the eastern margin of the Variscan Orogen, Bohemian Massif, Czech Republic. Am J Sci 305:407–448

Schulmann K, Konopásek J, Janoušek V, Lexa O, Lardeaux JM, Edel JB, Štípská P, Ulrich S (2009) An Andean type Palaeozoic convergence in the Bohemian Massif. Comptes Rendus Geosci 341:266–286

Siebel W, Chen F, Satir M (2003) Late-Variscan magmatism revisited: New implications from Pb-evaporation zircon ages on the emplacement of redwitzites and granites in NE Bavaria. Int J Earth Sci 92:36–53

Siebel W, Blaha U, Chen F, Rohrmüller J (2005a) Geochronology and geochemistry of a dyke-host rock association and implications for the formation of the Bavarian Pfahl shear zone, Bohemian Massif. Int J Earth Sci 94:8–23

Siebel W, Reitter E, Wenzel T, Blaha U (2005b) Sr isotope systematics of K-feldspars in plutonic rocks revealed by the Rb–Sr microdrilling technique. Chem Geol 222:183–199

Siebel W, Shang CK, Reitter E, Rohrmüller J, Breiter K (2008) Two distinctive granite suites in the SW Bohemian Massif and their record of emplacement: constraints from geochemistry and zircon $^{207}Pb/^{206}Pb$ chronology. J Petrol 49:1853–1872

Siebel W, Schmitt AK, Danišík M, Chen F, Meier S, Weiß S, Eroğlu S (2009) Prolonged mantle residence of zircon xenocrysts from the western Eger rift. Nat Geosci 2:886–890

Sláma J, Košler J, Condon DJ, Crowley JL, Gerdes A, Hanchar JM, Horstwood MSA, Morris GA, Nasdala L, Norberg N, Schaltegger U, Schoene B, Tubrett MN, Whitehouse MJ (2008) Plešovice zircon—a new natural reference material for U–Pb and Hf isotopic microanalysis. Chem Geol 249:1–35

Soman A, Geisler T, Tomaschek F, Grange M, Berndt J (2010) Alteration of crystalline zircon solid solutions: a case study from an alkaline pegmatite from Zomba-Malosa, Malawi. Contrib Miner Petrol 160:909–930

Teipel U, Rohrmüller H, Eichhorn R, Höll R, Wamsler S, Kennedy A (2002) U-Pb-SHRIMP-Datierungen an Zirkonen von leukokraten Gneisen und eines Metabasits aus dem Bayerischen Wald (westliche Böhmische Masse). Pangeo Austria 2002:175–176

Teipel U, Eichhorn R, Loth G, Rohrmüller J, Höll R, Kennedy A (2004) U–Pb SHRIMP and Nd isotopic data from the western Bohemian Massif (Bayerischer Wald, Germany): implications for Upper Vendian and Lower Ordovician magmatism. Int J Earth Sci 93:782–801

Vavra G, Schmid R, Gebauer D (1999) Internal morphology, habit and U–Th–Pb microanalysis of amphibolite-to-granulite facies zircons: geochronology of the Ivrea Zone (Southern Alps). Contrib Miner Petrol 134:380–404

Watson EB, Harrison TM (1983) Zircon saturation revisited: temperature and composition effects in a variety of crustal magma types. Earth Planet Sci Lett 64:295–304

Wendt JI, Kröner A, Fiala J, Todt W (1994) U–Pb Zircon and Sm–Nd dating of Moldanubian HP/HT granulites from south Bohemia, Czech Republic. J Geol Soc Lond 151:83–90

Whitehouse MJ, Platt JP (2003) Dating high-grade metamorphism—constraints from rare-earth elements in zircon and garnet. Contrib Miner Petrol 145:61–74

Wilde SA, Valley JW, Peck WH, Graham CM (2001) Evidence from detrital zircons for the existence of continental crust and oceans on the Earth 4.4 Gyr ago. Nature 409:175–178

Zeck HP, Williams IS (2002) Inherited and magmatic zircon from Neogene Hoyazo cordierite dacite, SE Spain—anatectic source rock provenance and magmatic evolution. J Petrol 43:1089–1104